Earth, Planets and Space
a SpringerOpen Journal

FULL PAPER Open Access

A simulation study of the propagation of whistler-mode chorus in the Earth's inner magnetosphere

Yuto Katoh

Abstract

We study the propagation of whistler-mode chorus in the magnetosphere by a spatially two-dimensional simulation code in the dipole coordinates. We set the simulation system so as to assume the outside of the plasmapause, corresponding to the radial distance from 3.9 to 4.1 R_E in the equatorial plane and the latitudinal range from −15° to +15°, where R_E is the Earth's radius. We assume a model chorus element propagating northward from the magnetic equator of the field line at $L = 4$ with a rising tone from 0.2 to 0.7 Ω_{e0} in the time scale of 5,000 Ω_{e0}^{-1}, where Ω_{e0} is the electron gyrofrequency at the magnetic equator. For the initial density distribution of cold electrons, we assume three types of initial conditions in the outside of the plasmapause: without a duct (run 1), a density enhancement duct (run 2), and a density decrease duct (run 3). In run 1, the simulation result reveals that whistler-mode waves of the different wave frequencies propagate in the different ray path in the region away from the magnetic equator. In runs 2 and 3, the model chorus element propagates inside the assumed duct with changing wave normal angle. The simulation results show the different propagation properties of the chorus element in runs 2 and 3 and reveal that resultant wave spectra observed along the field line are different between the density enhancement and density decrease duct cases. The spectral modification of chorus by the propagation effect should play a significant role in the interactions between chorus and energetic electrons in the magnetosphere, particularly in the region away from the equator. The present study clarifies that the variation of propagation properties of chorus should be taken into account for the thorough understanding of resonant interactions of chorus with energetic electrons in the inner magnetosphere.

Keywords: Whistler-mode waves; Magnetosphere; Numerical experiments; Dipole geometry

Background

Whistler-mode chorus emissions are generated in the region close to the magnetic equator outside the plasmapause during geomagnetically disturbed periods. Spacecraft observations near the magnetic equator have revealed that chorus appear in the frequency range from 0.2 to 0.8 Ω_{e0}, where Ω_{e0} is the electron gyrofrequency at the magnetic equator, while the frequency range of chorus is classified into the lower-band (0.2 to 0.5 Ω_{e0}) and upper-band chorus (0.5 to 0.8 Ω_{e0}) by a distinct gap at 0.5 Ω_{e0} (Santolík et al. 2003). Observations have revealed that chorus typically propagate along a magnetic field line in its source region and become oblique during their propagation away from the equator. Propagation properties of chorus have been studied for a half of century (e.g., Smith et al. 1960; Bell et al. 2009). Theoretical estimations and results of ray tracing studies have been compared with observations of chorus in space and at high-latitude ground stations.

Chorus can resonate with electrons in a wide energy range from kiloelectron volts to megaelectron volts and play important roles in the energization process of radiation belt electrons (e.g., Katoh et al. 2008) and in the auroral electron precipitation process related to pulsating aurora (e.g., Nishiyama et al. 2011). Propagation properties of chorus are important in understanding resonant interactions with energetic electrons. While whistler-mode waves propagating parallel to the magnetic field direction are circularly polarized waves with purely electromagnetic components, interactions can be treated based on the cyclotron resonance condition. For a

Correspondence: yuto@stpp.gp.tohoku.ac.jp
Department of Geophysics, Graduate School of Science, Tohoku University, 6-3 Aramaki-aza-aoba, Aoba, Sendai, Miyagi 980-8578, Japan

case of obliquely propagating whistler-mode waves, their wave electromagnetic fields exhibit longitudinal components, and the Landau resonance with energetic electrons becomes significant. The propagation properties of chorus are governed by the spatial distribution of ambient cold electrons controlling the dispersion relation of plasma waves. Previous studies have revealed conditions of trapping of whistler-mode waves within enhanced or depleted plasma density (Bell et al. 2009).

The generation process of chorus has been reproduced by self-consistent particle simulations (Katoh and Omura 2007; 2011; 2013). Since a spatially one-dimensional simulation system along a magnetic field line has been used in these simulations, whistler-mode waves of purely parallel propagation are treated. While essential processes of the chorus generation occurring in the region close to the magnetic equator can be well described by the assumption of the parallel propagation, observation results have revealed that generated chorus elements become oblique and propagate across field lines in the region away from the equator (e.g., Santolík et al. 2003). For the discussion of the propagation of chorus in the magnetosphere, we need to develop a spatially two-dimensional simulation code which enables us to treat whistler-mode waves propagating in arbitrary directions.

Ray tracing is a useful tool to understand propagation properties of chorus in the magnetosphere (Kimura 1966; Bortnik et al. 2008; Yamaguchi et al. 2013). Numerical experiments are also useful, even though an amount of computational resources are required in solving a set of Maxwell's equations and the equation of motion of cold plasma, because they can reproduce the wave amplitude variation and the spatial extent of wave packets during their propagation (Streltsov et al. 2006, 2010, 2012). In the present study, we have developed a spatially two-dimensional simulation code for the study of the propagation of chorus in the dipole magnetic field. We show the validity of the developed simulation code and study variations of propagation properties of chorus by assuming the density enhancement and decrease in the magnetosphere. Simulation results also reveal that spectra of rising tone chorus are significantly modified during the propagation of chorus in the region away from the equator. The present study clarifies that the variation of propagation properties of chorus should be taken into account for the thorough understanding of resonant interactions of chorus with energetic electrons in the inner magnetosphere. We describe the simulation model in the 'Methods' section. In the 'Results and discussion' section, we present simulation results and discuss the propagation properties of chorus in the simulation results. The 'Conclusions' section gives a summary of the present study.

Methods

We solve the equation of motion of a cold electron fluid and Maxwell's equations for the evolution of electromagnetic fields in the simulation system:

$$\frac{\partial \boldsymbol{V}}{\partial t} = -\boldsymbol{V}\cdot\nabla\boldsymbol{V} + \frac{q_e}{m_e}\left(\boldsymbol{E} + \boldsymbol{V}\times\boldsymbol{B}\right), \tag{1}$$

$$\frac{\partial N}{\partial t} = -\nabla\cdot\left(N\boldsymbol{V}\right), \tag{2}$$

$$\frac{\partial \boldsymbol{B}}{\partial t} = -\nabla\times\boldsymbol{E}, \tag{3}$$

$$\frac{\partial \boldsymbol{E}}{\partial t} = \frac{1}{\varepsilon_0\mu_0}\nabla\times\boldsymbol{B} - \frac{1}{\varepsilon_0}\boldsymbol{J}, \tag{4}$$

and

$$\boldsymbol{J} = q_e N\boldsymbol{V}, \tag{5}$$

where q_e and m_e are the charge and the rest mass of an electron, respectively, and N is the number density of electrons. While we assume that ions are stationary neutralizing background, Equation 2 enables us to treat the deviation of the spatial distribution of a cold electron fluid from the equilibrium. Although the contribution of Equation 2 would be negligible in the present study because the assumed wave amplitude is not so large, the density perturbation of cold electrons should be significant for the case of large-amplitude oblique whistler-mode waves, as has been studied by Yoon (2011). The velocity vector $\boldsymbol{V}$ of cold electrons and wave electromagnetic field vectors $\boldsymbol{E}$ and $\boldsymbol{B}$ are defined in the Cartesian coordinate (X, Y, Z), where the Z axis is defined in the antiparallel direction of the dipole moment and the X and Y axes are orthogonal to the Z axis and are defined in the equatorial plane. We solve this set of equations in the dipole coordinate system (h, ν, ϕ), which is defined through the spherical coordinates (r, θ, ϕ) as

$$h = -\frac{\sinh^{-1}\left(a\cos\theta/r^2\right)}{\sinh^{-1}a} \tag{6}$$

and

$$\nu = \frac{r}{\sin^2\theta}, \tag{7}$$

where the h axis is along a magnetic field line, the ν axis is perpendicular to the h axis and is defined in the meridional plane, the ϕ axis completes the right-hand system, and a is a constant related to the grid distribution along a field line.

We compute the equations in the computational domain, which is projected onto the physical domain using metric terms (cf. Kageyama 2006), as shown in Figure 1. We assume a spatially two-dimensional simulation system in the $h-\nu$ meridional plane corresponding to the range of the radial distance from 3.9 to 4.1 R_E at the magnetic equator and the latitudinal range from $-15°$ to $+15°$, where R_E is the Earth's radius. The

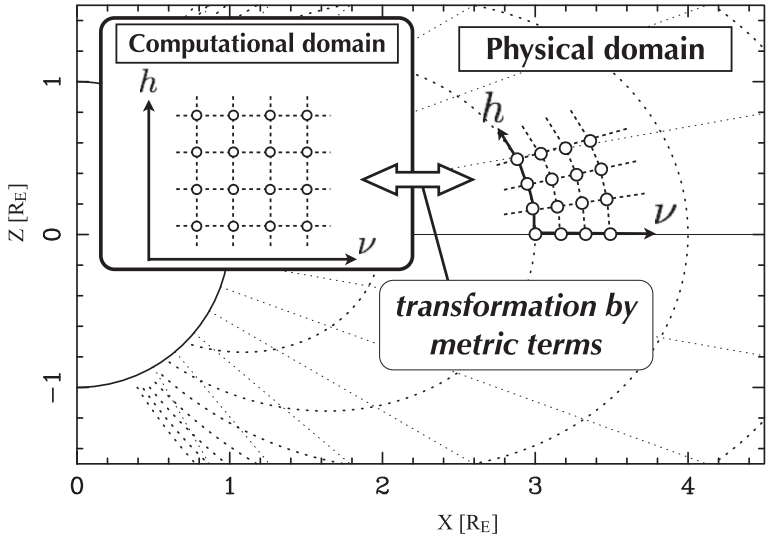

Figure 1 Schematic of the simulation system.

number of grid points used in the present study is 20,480 for h and 1,024 for v. In order to realize an open boundary condition, we assume damping regions at the edges of the simulation system as we used in our previous studies (e.g., Katoh and Omura 2006) by a masking method after Umeda et al. (2001).

The intensity of the background magnetic field varies in the simulation system according to the dipole field, as shown in Figure 2a. Figure 2b shows the spatial distribution of cold electrons in the simulation system. We assume that the radial distribution of the number density of cold electrons at the magnetic equator is given by

$$N_{\mathrm{eq}}(r_{\mathrm{eq}}) = 9\,N_0 \exp\left\{-\frac{(r_{\mathrm{eq}} - r_0)^2}{\Delta r_{\mathrm{pp}}}\right\} + N_{\mathrm{eq,min}}, \qquad (8)$$

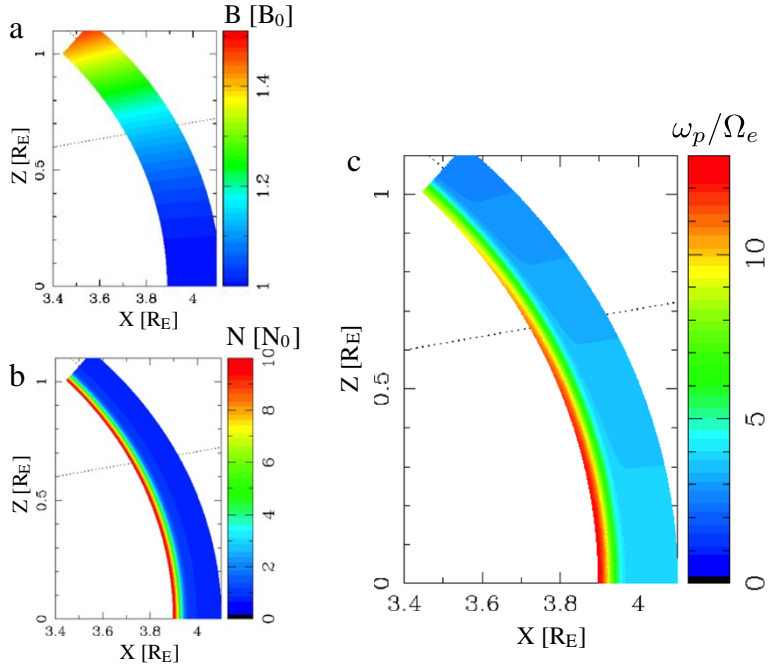

Figure 2 Spatial distribution of (a) the intensity of the background magnetic field, (b) the number density of cold electrons, and (c) ω_p/Ω_e.

where N_0 is the number density at the magnetic equator of the magnetic field line of $L = 4$, r_0 represents the location of the inner edge of the simulation system at the magnetic equator and is 3.9 R_E from the center of the Earth, Δr_{pp} is the spatial scale of the density gradient at the plasmapause and is assumed to be 0.033 R_E, and $N_{eq,min}$ is the minimum of the equatorial number density. In Figure 2b, we assume $N_{eq,min} = N_0$. The spatial distribution of the number density in the region away from the equator is determined by referring $N_{eq}(r_{eq})$ and the diffusive equilibrium along a magnetic field line (Angerami and Thomas 1964). We obtain the ratio between the plasma frequency and the electron gyrofrequency, ω_p/Ω_e, by the dipole magnetic field and the assumed spatial distribution of cold electrons, as shown in Figure 2c. We assume N_0 so that ω_p/Ω_e becomes 4.0 at the magnetic equator of $L = 4$.

Results and discussion

Using the simulation model described in the previous section, we study the propagation of whistler-mode waves with a rising tone in the inner magnetosphere. We inject northward propagating whistler-mode waves from the magnetic equator of the field line at $L = 4$ with varying its frequency in time, as a model chorus element. The wave frequency is varied from 0.2 to 0.7 Ω_{e0} with the time scale of 5,000 Ω_{e0}^{-1}. The assumed frequency range covers the entire frequency range of typical lower-band and upper-band chorus emissions, and the time scale and the frequency sweep rate of the rising tone correspond to 58 ms and 117 kHz/s, respectively, for the magnetic field intensity of 486 nT at the equator of $L = 4$. The assumed time scale is comparable to those of typical chorus emissions (Santolík et al. 2003), while the assumed sweep rate is a few times higher than typical sweep rates. The wave amplitude of the model chorus element is assumed to be $10^{-4}\,B_0$, where B_0 is the intensity of the background magnetic field at the magnetic equator of $L = 4$. We study propagation properties of the model chorus element under three types of background plasma conditions: outside of the plasmapause (run 1), a density enhancement (run 2), and a density decrease (run 3).

Run 1: propagation of a rising tone chorus element outside the plasmapause

Figure 3 shows the distribution of the wave magnetic field amplitude at (a) $t = 1,250\,\Omega_{e0}^{-1}$, (b) $10,000\,\Omega_{e0}^{-1}$, (c) $15,000\,\Omega_{e0}^{-1}$, and (d) $20,000\,\Omega_{e0}^{-1}$. Figure 4 represents the estimated wave normal angle of the waves at the same time intervals of the results shown in Figure 3. The injected model chorus element propagated along the field line of $L = 4$ (Figures 3a and 4a). At the magnetic latitude around 10°, the waves deviated outward from the field line (Figure 3b) with changing their wave normal angle oblique, approximately 60° (Figure 4b), as has been reported in previous observations. On the other hand, the wave component of the higher frequency range (>0.5 Ω_{e0}) slightly deviated inward from the magnetic field line (Figures 3c,d and 4c,d). The different ray path of whistler-mode waves depending on the wave frequency has also

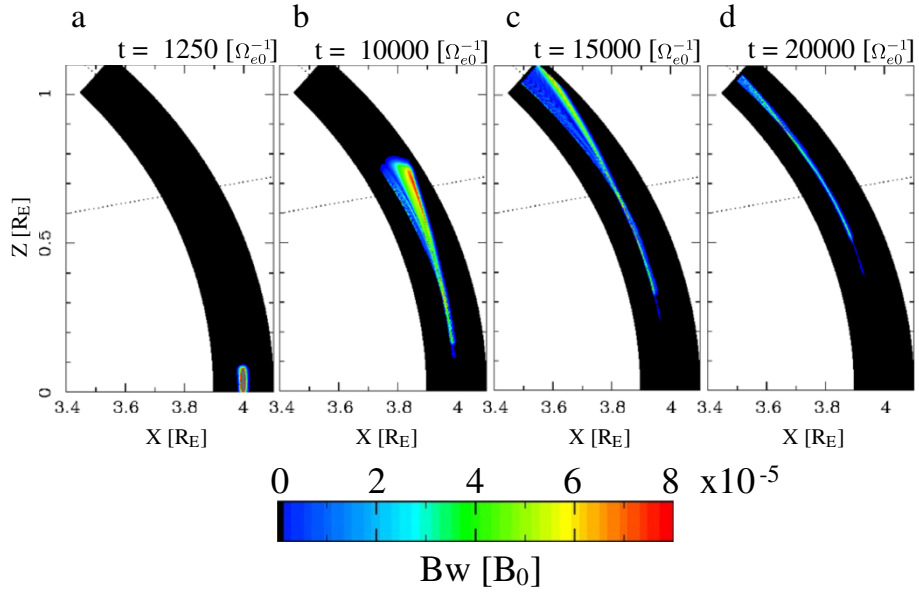

Figure 3 Spatial distribution of the wave magnetic field amplitude at (a) $t = 1,250\,\Omega_{e0}^{-1}$, (b) $t = 10,000\,\Omega_{e0}^{-1}$, (c) $t = 15,000\,\Omega_{e0}^{-1}$, and (d) $t = 20,000\,\Omega_{e0}^{-1}$.

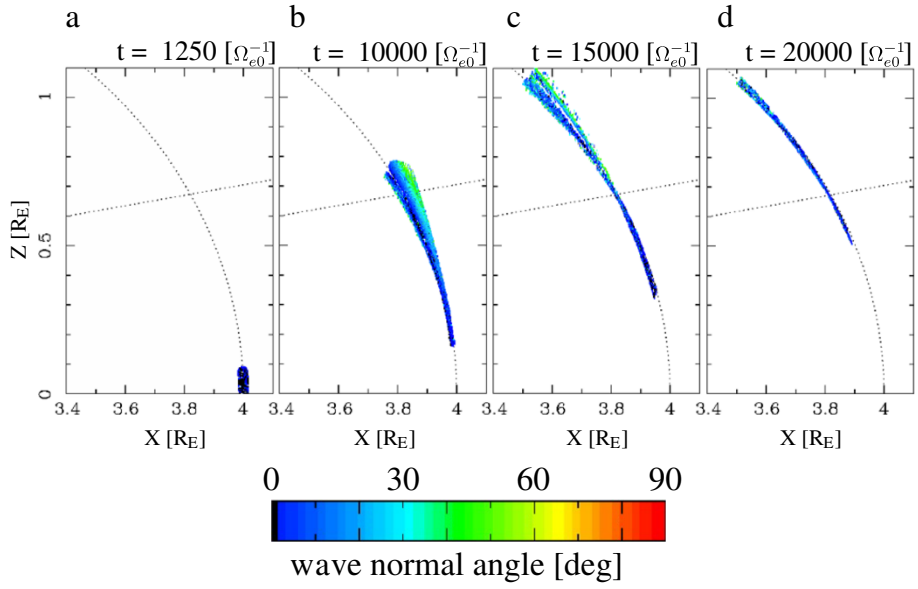

Figure 4 Spatial distribution of the wave normal angle of the waves at (a) $t = 1,250\ \Omega_{e0}^{-1}$, (b) $t = 10,000\ \Omega_{e0}^{-1}$, (c) $t = 15,000\ \Omega_{e0}^{-1}$, and (d) $t = 20,000\ \Omega_{e0}^{-1}$.

been pointed out by ray trace analyses (Yamaguchi et al. 2013), and the result of the present study is consistent with those of the previous studies. The deviation of the model chorus element from the magnetic field line of $L = 4$ can also be identified by the wave spectra measured along the field line. Figure 5 shows the time evolution of spectra along the field line. The model chorus element covering in the frequency range from 0.2 to 0.7 Ω_{e0} appears in the spectra at $t = 5,000\ \Omega_{e0}^{-1}$ (Figure 5a), but both higher and lower frequency components of the element weakened

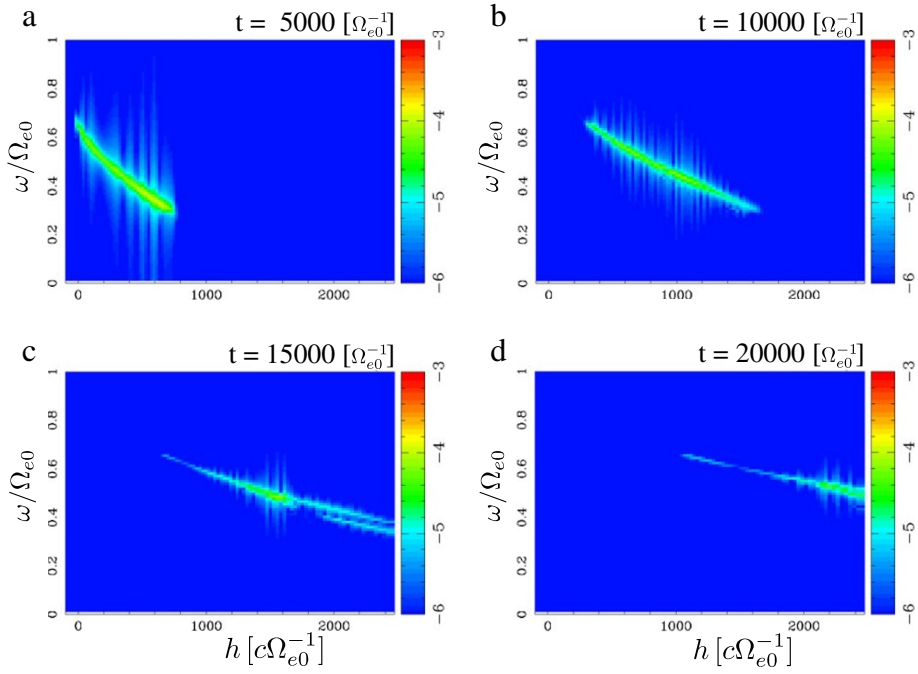

Figure 5 Spatial distribution of the wave spectra measured along the field line of $L = 4$ at (a) $t = 5,000\ \Omega_{e0}^{-1}$, (b) $t = 10,000\ \Omega_{e0}^{-1}$, (c) $t = 15,000\ \Omega_{e0}^{-1}$, and (d) $t = 20,000\ \Omega_{e0}^{-1}$.

during their propagation (Figures 5b,c,d), because of the outward and inward deviations of the higher and lower frequency components of the element.

Runs 2 and 3: duct propagation of a rising tone chorus element

Next, we consider the duct propagation of the model chorus element. We use the same model chorus element as shown in the previous section. The propagation of whistler-mode waves along a field line of the density enhancement or density decrease has been studied for decades (e.g., Smith et al. 1960). The propagation properties of whistler-mode chorus have also been discussed by theories (e.g., Bell et al. 2009) and observations (e.g., Haque et al. 2011) for the explanation of the spectral gap at half the gyrofrequency dividing chorus emissions into upper band and lower band. Figure 6 shows the radial distribution of the background cold electrons at the magnetic equator of the simulation system. We assume the density profile so that ω_p/Ω_e becomes 4.0 at the equator of $L = 4$ and the width of the density variation corresponds to the spatial scale of the generation region (approximately 100 km) of chorus emissions in the inner magnetosphere (Santolík et al. 2003).

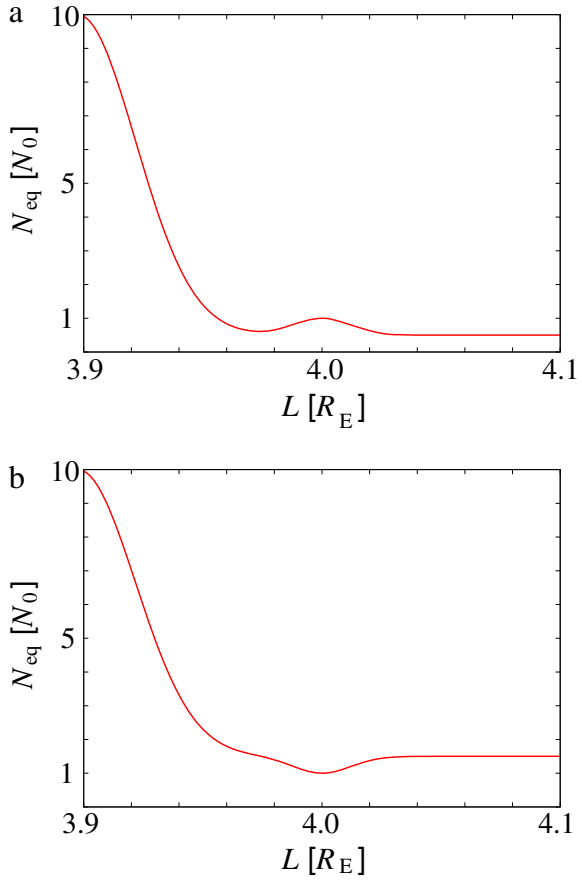

Figure 6 Radial profiles of the background cold electrons at the equator of the simulation system. For the cases of **(a)** the density enhancement and **(b)** the density decrease.

Figure 7a,b,c,d shows the time evolution of the spatial distribution of the wave magnetic field in run 2. In Figure 7a, we find that the model chorus element is generated at the equator and is propagating away from the equator. The element propagated fairly along the magnetic field line of $L = 4$ without significant deviation as we found in the previous section. Figure 8a,b,c,d represents the wave normal angle of the waves in the simulation system. These results show that the wave element varies its wave normal angle during the propagation and that the amount of the variation is within 30°. The wave normal angle did not increase significantly even the wave element reached the region of the magnetic latitude larger than 10°.

Figure 7e,f,g,h shows the time evolution of the wave magnetic field amplitude in the simulation system for the case of the density decrease (run 3). We find that the model chorus element propagated along the field line of $L = 4$, similar to the results shown in Figure 7a,b,c,d, while the wave amplitude slightly enhanced at the leading edge in the case of the density decrease. Figure 8e,f,g,h shows the wave normal angle of the waves. As we found in the case of the density enhancement, the wave normal angle of the element varied within the limited range during its propagation away from the equator.

The propagation characteristics of the wave element is explained by the properties of ducting whistler-mode waves (Smith et al. 1960). Figure 9 is the zoomed plot of the equatorial region of Figures 7a and 8a of run 2 and Figures 7e and 8e of run 3. As has been discussed in previous studies, whistler-mode waves are propagating around the center of the duct for the density enhancement case, while waves are reflecting between the edges of the density decrease duct. Because of this propagation property, the chorus element emitted from the magnetic equator is guided along the field line of $L = 4$ in both density enhancement and decrease cases. The different propagation properties between these cases shown in Figure 9 resulted in the difference of the time scale of propagation. The leading edge of the wave element propagated over 10° of latitude at $t = 10,000\,\Omega_{e0}^{-1}$ for the density enhancement case (Figure 7b), while the wave element did not reach for the density decrease case (Figure 7f), because of the different ray path lengths of the wave elements.

The propagation properties of whistler-mode waves in the magnetosphere under the presence of the density gradient have also been studied in Woodroffe and Streltsov (2013a,b). The properties of the wave propagation shown in the present simulation results are consistent with those reported in the previous works. By employing a large

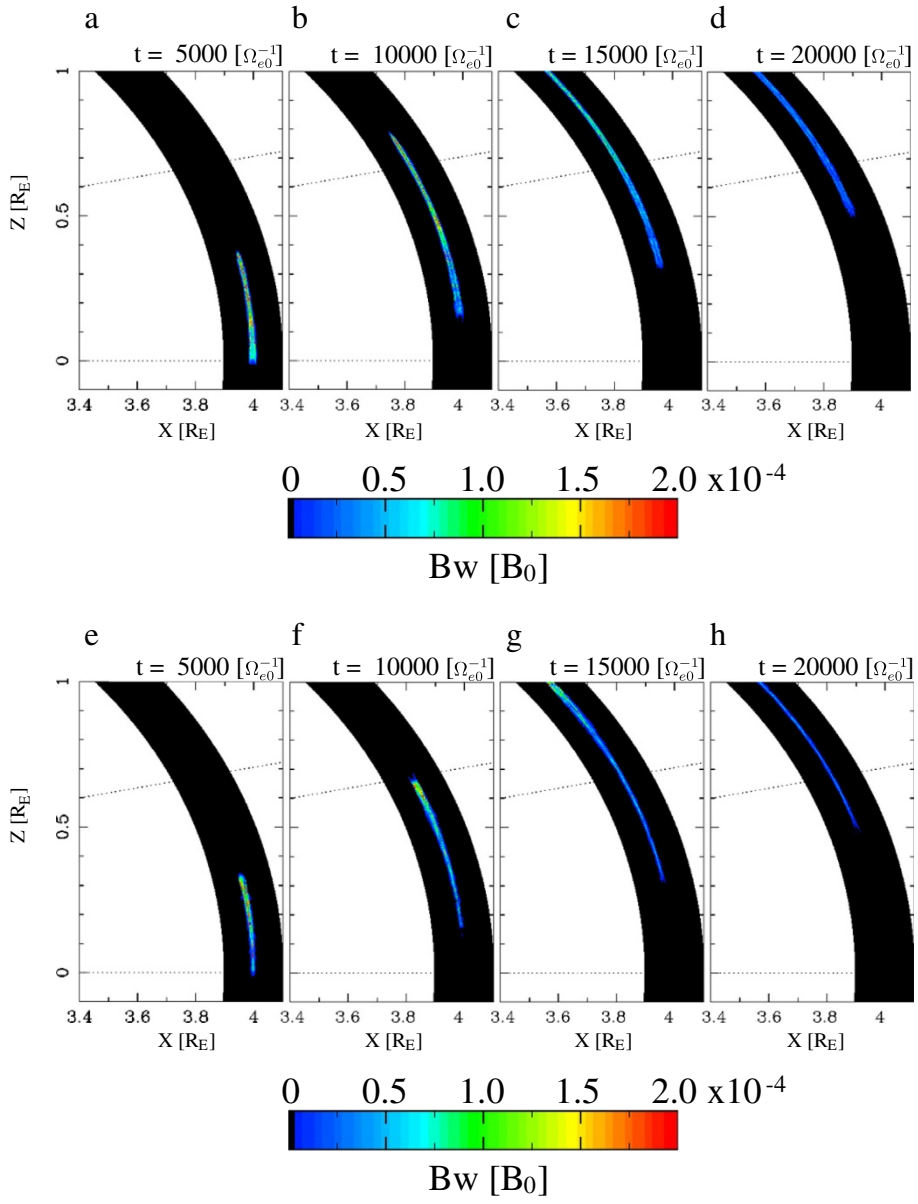

Figure 7 Spatial distribution of the wave magnetic field amplitude. At **(a)** $t = 5,000\,\Omega_{e0}^{-1}$, **(b)** $t = 10,000\,\Omega_{e0}^{-1}$, **(c)** $t = 15,000\,\Omega_{e0}^{-1}$, and **(d)** $t = 20,000\,\Omega_{e0}^{-1}$ for the density enhancement case and **(e-h)** those for the density decrease case, respectively.

simulation system compared with those used in the previous studies (the system is four times and ten times larger in the Z and X directions, respectively, than that used in Woodroffe and Streltsov (2013b)), we have demonstrated in the present study how the wave spectra are modified by the propagation effect.

The properties of the duct propagation modify the wave spectra measured along the field line, and the modification appears differently in runs 2 and 3. In Figure 10, we show the time evolution of the spectra obtained along the field line of $L = 4$. Since the wave element is guided along the assumed density structure with slight deviation from the field line, the spectra show an amplitude modulation similar to sub-packet structures of chorus (Santolík et al. 2003). We also found that the amplitude modulation of the spectra is different in runs 2 and 3. Figure 11 shows the maximum wave amplitude at each frequency bin of Figure 10b (run 2) and Figure 10f (run 3). The frequency width of the amplitude modulation is relatively smaller in run 2 than in run 3. These results show that, even if the amplitude of waves generated at the magnetic equator is constant, the spectra of the waves are significantly

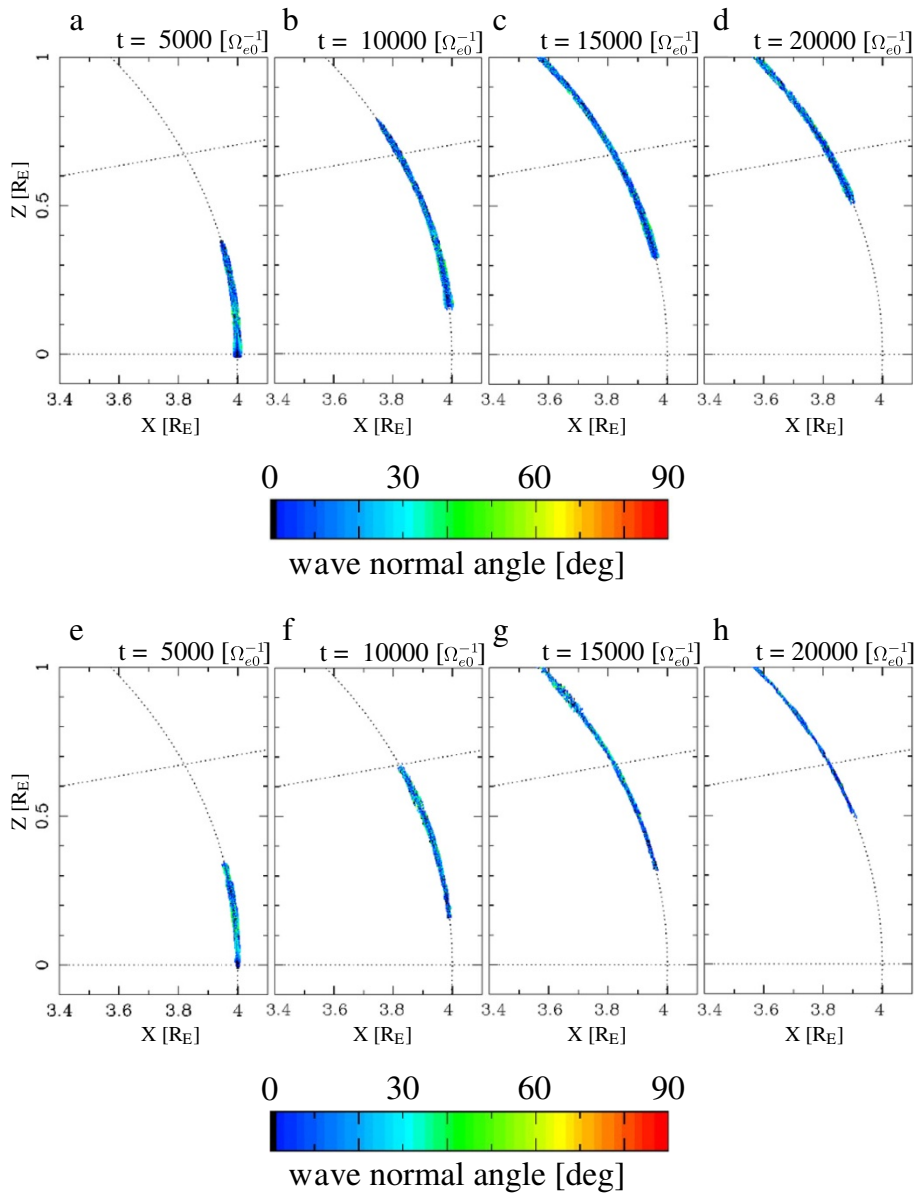

Figure 8 Spatial distribution of the wave normal angle of the waves. At **(a)** $t = 5,000\ \Omega_{e0}^{-1}$, **(b)** $t = 10,000\ \Omega_{e0}^{-1}$, **(c)** $t = 15,000\ \Omega_{e0}^{-1}$, and **(d)** $t = 20,000\ \Omega_{e0}^{-1}$ for the density enhancement case and **(e-h)** those for the density decrease case, respectively.

modulated by the propagation effect. Since chorus elements generated in the region close to the magnetic equator intrinsically show sub-packet structures in the spectra, the results of the present study reveal that wave spectra measured by satellites in the region away from the equator should be formed by a combination of the intrinsic spectra and the spectral modulation by the propagation effect.

Santolík et al. (2003) showed Cluster observation that chorus propagate nearly parallel to the field lines in the region close to the magnetic equator and the average wave vector directions gradually become inclined at higher latitudes (approximately 10°). The present simulation results shown in Figure 4 are consistent with the observation results. Li et al. (2011) studied the relationship between the amplitude of chorus and the density variations observed by THEMIS spacecraft. They showed that both density enhancement and density decrease are correlated with increases of wave amplitude, depending on the local time of the observation. While they proposed the modulation of the linear growth rate as a potential mechanism, the suggested relationship between the

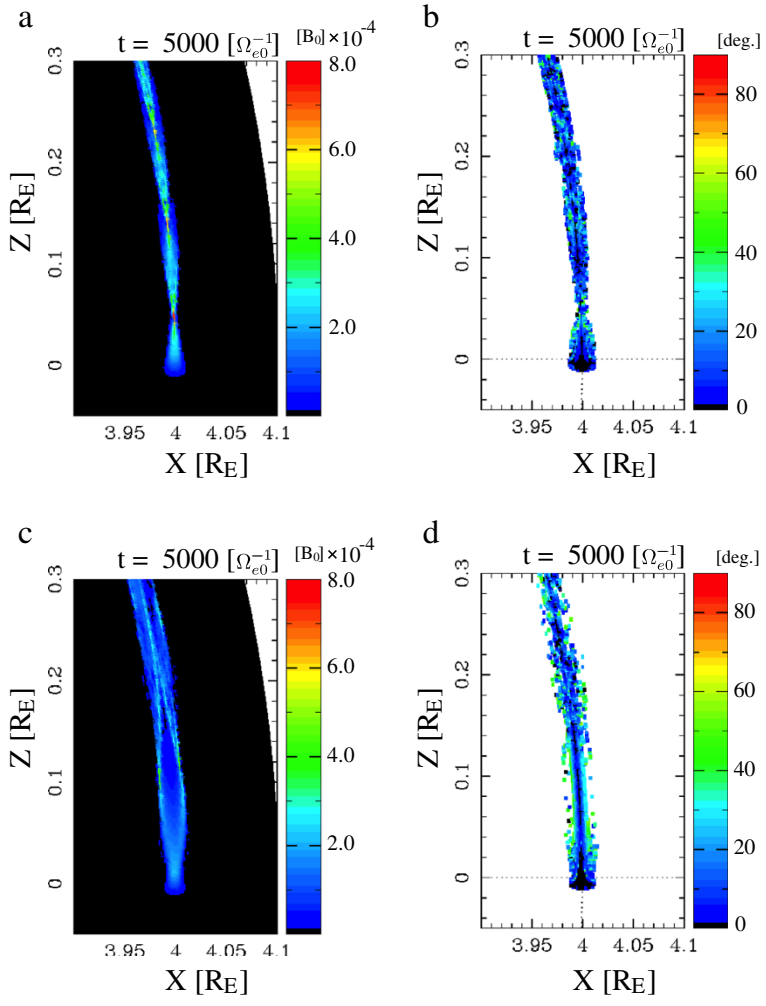

Figure 9 Zoomed plot of the spatial distributions. (a) The wave magnetic field amplitude and **(b)** wave normal angle around the equator for the case of density enhancement at $t = 5,000\,\Omega_{e0}^{-1}$ and **(c, d)** those for the case of density decrease, respectively.

wave amplitude and the density distribution might be explained by the propagation effect as discussed in the present study. We expect fruitful discussions by comparing observation of chorus with results of the present simulation.

We expect that the spectral modification by the propagation effect revealed by the present study plays a significant role in the resonant scattering process between chorus and energetic electrons in the magnetosphere. While energetic electrons are bouncing along a field line and resonate with a chorus element, for the case of the duct propagation, the time scale of the interaction is controlled by the spatial scale of ducts. If the spatial scale of ducts is comparable to the gyroradius of energetic electrons, since the deviation of the wave packet from the field line is small during the propagation, electrons can resonate with the entire wave element of chorus. On the other hand, if the spatial scale of ducts is larger than the gyroradius, the wave element often deviates from the field line and the electrons only interact with a part of the wave element, resulting in the limited time scale of resonant interactions. The present study clarified that the variation of propagation properties of chorus should be taken into account for the thorough understanding of resonant interactions of chorus with energetic electrons in the inner magnetosphere. The same discussion can also be applied to the acceleration of relativistic electrons in the outer radiation belt, since the concentration of wave amplitude within the duct should affect the time scale of wave-particle interactions between chorus and relativistic electrons. It is interesting to evaluate the efficiency of the acceleration by computing the motion of relativistic electrons simultaneously with the present simulation.

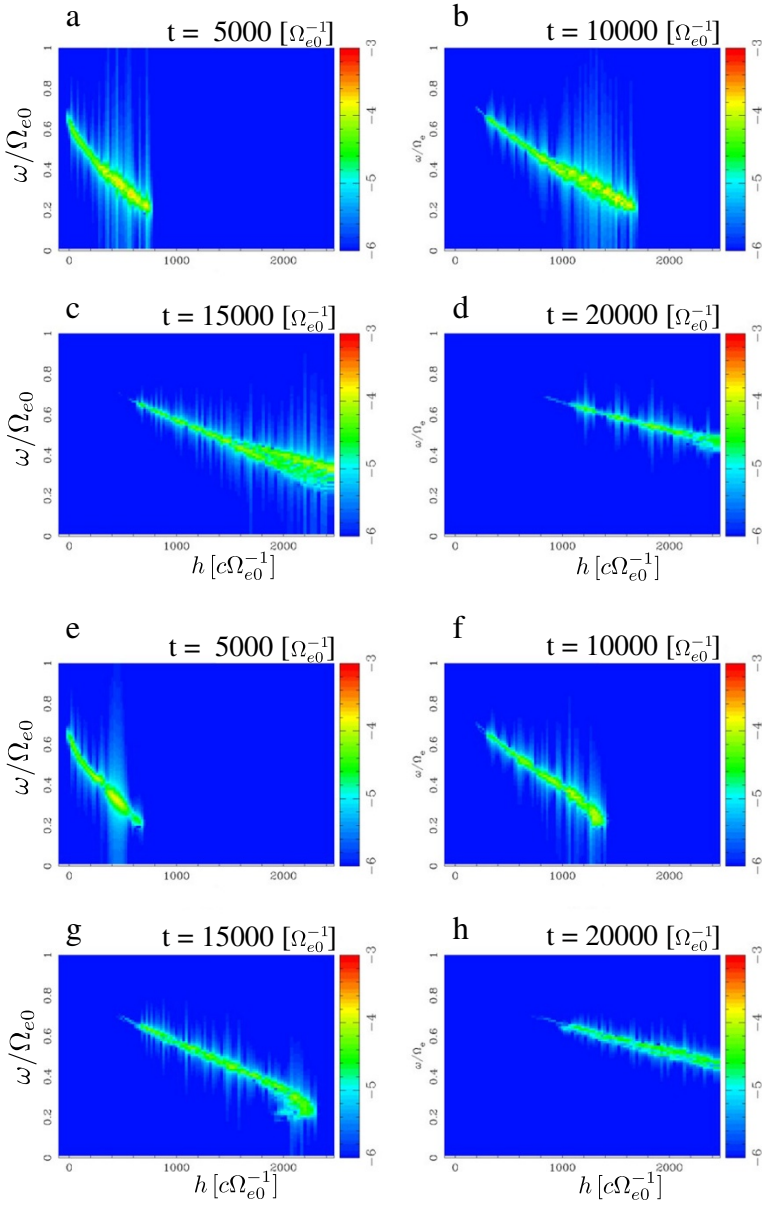

Figure 10 Spatial distribution of the wave spectra measured along the field line of $L = 4$. At **(a)** $t = 5,000\ \Omega_{e0}^{-1}$, **(b)** $t = 10,000\ \Omega_{e0}^{-1}$, **(c)** $t = 15,000\ \Omega_{e0}^{-1}$, and **(d)** $t = 20,000\ \Omega_{e0}^{-1}$ for the density enhancement case, and **(e-h)** those for the density decrease case, respectively.

Conclusions

We developed a spatially two-dimensional simulation code in the dipole coordinates (h,v) for the study of the propagation of whistler-mode chorus in the magnetosphere. We set the simulation system so as to simulate the outside of the plasmapause, corresponding to the radial distance from 3.9 to 4.1 R_E in the equatorial plane and the latitudinal range from $-15°$ to $+15°$. We assumed a model chorus element propagating northward from the magnetic equator of the field line of $L = 4$ with a rising tone from 0.2 to 0.7 Ω_{e0} in the time scale of 5,000 Ω_{e0}^{-1}. For the density distribution of cold electrons, we assumed three types of initial conditions in the outside of the plasmapause: without a duct (run 1), a density enhancement duct (run 2), and a density decrease duct (run 3). In run 1, the simulation result revealed that whistler-mode waves of different wave frequencies propagated in the different ray path in the region away from the magnetic equator. In runs 2 and 3, we found that the model chorus element propagated inside the assumed duct with changing wave normal angle. The simulation results showed the different propagation properties of the chorus element in runs

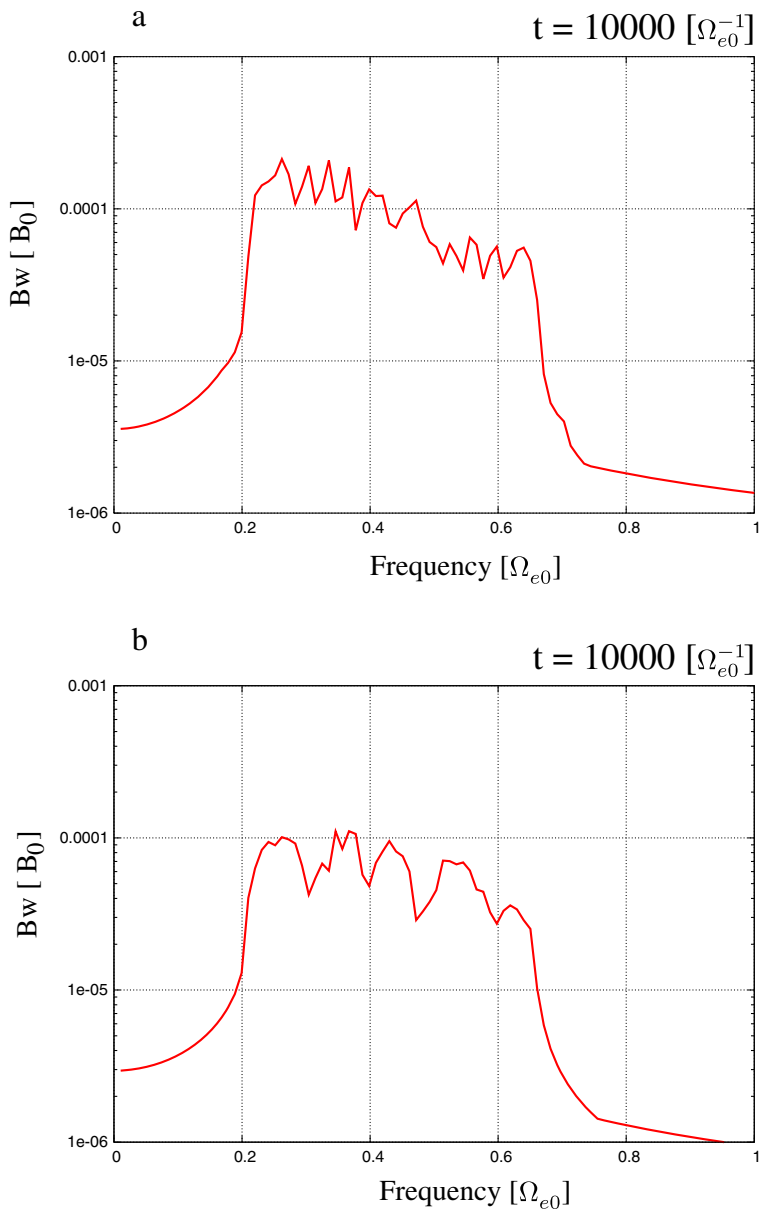

Figure 11 Maximum wave amplitude as a function of the wave frequency observed along the field line of $L = 4$. At $t = 10,000\,\Omega_{e0}^{-1}$ for the case of **(a)** density enhancement and **(b)** density decrease.

2 and 3 and revealed that resultant wave spectra observed along the field line were different between the density enhancement and density decrease duct cases.

The spectral modification of chorus by the propagation effect should play a significant role in the interactions between chorus and energetic electrons in the magnetosphere, particularly in the region away from the equator. For the quantitative evaluation of the effect of the propagation properties on the resonant scattering process, the motion of energetic electrons should be computed simultaneously with the present simulation. We leave them for the future study.

Competing interests
The author declares that he has no competing interests.

Acknowledgements
The author thanks N. Terada for the discussion on the implementation of the dipole coordinates in the simulation code. The computation was performed with computer facilities at Research Institute for Sustainable Humanosphere and Academic Center for Computing and Media Studies of Kyoto University, Solar-Terrestrial Environment Laboratory of Nagoya University, and Research Institute for Information Technology of Kyushu University. This work was supported by Grant for Young Scientist of Graduate School of Science, Tohoku University.

Received: 3 February 2014 Accepted: 11 March 2014
Published: 7 April 2014

References

Angerami JJ, Thomas JO (1964) Studies of planetary atmospheres: 1. The distribution of ions and electrons in the Earth's exosphere. J Geophys Res 69: 4537–4560. doi:10.1029/JZ069i021p04537.

Bell TF, Inan US, Haque N, Pickett JS (2009) Source regions of banded chorus. Geophys Res Lett 36: L11101. doi:10.1029/2009GL037629.

Bortnik J, Thorne RM, Meredith NP (2008) The unexpected origin of plasmaspheric hiss from discrete chorus emissions. Nature 452: 62–66. doi:10.1038/nature06741.

Haque N, Inan US, Bell TF, Pickett JS, Trotignon JG, Facskó G (2011) Cluster observations of whistler mode ducts and banded chorus. Geophys Res Lett 38: L18107. doi:10.1029/2011GL049112.

Katoh Y, Omura Y (2006) A study of generation mechanism of VLF triggered emission by self-consistent particle code. J Geophys Res 111: A12207. doi:10.1029/2006JA011704.

Katoh, Y, Omura Y (2007) Computer simulation of chorus wave generation in the Earth's inner magnetosphere. Geophys Res Lett 34: L03102. doi:10.1029/2006GL028594.

Katoh Y, Omura Y, Summers D (2008) Rapid energization of radiation belt electrons by nonlinear wave trapping. Ann Geophys 26: 3451–3456

Katoh Y, Omura Y (2011) Amplitude dependence of frequency sweep rates of whistler mode chorus emissions. J Geophys Res 116: A07201. doi:10.1029/2011JA016496.

Katoh, Y, Omura Y (2013) Effect of the background magnetic field inhomogeneity on generation processes of whistler-mode chorus and broadband hiss-like emissions. J Geophys Res Space Phys 118: 4189–4198. doi:10.1002/jgra.50395.

Kageyama A, Sugiyama T, Watanabe K, Sato T (2006) A note on the dipole coordinates. Comput Geosci 32: 265–269. doi:10.1016/j.cageo.2005.06.006.

Kimura I (1966) Effects of ions on whistler-mode ray tracing. Radio Sci 1: 269–283

Li W, Bortnik J, Thorne RM, Nishimura Y, Angelopoulos V, Chen L (2011) Modulation of whistler mode chorus waves: 2. Role of density variations. J Geophys Res 116: A06206. doi:10.1029/2010JA016313.

Nishiyama T, Sakanoi T, Miyoshi Y, Katoh Y, Asamura K, Okano S, Hirahara M (2011) The source region and its characteristic of pulsating aurora based on the Reimei observations. J Geophys Res 116: A03226. doi:10.1029/2010JA015507.

Santolík O, Gurnett DA, Pickett JS (2003) Spatio-temporal structure of storm-time chorus. J Geophys Res 108: 1278. doi:10.1029/2002JA009791.

Smith RL, Helliwell RA, Yabroff IW (1960) A theory of trapping of whistlers in field-aligned columns of enhanced ionization. J Geophys Res 65: 815–823. doi:10.1029/JZ065i003p00815.

Streltsov AV, Lampe M, Manheimer W, Ganguli G, Joyce G (2006) Whistler propagation in inhomogeneous plasma. J Geophys Res 111: A03216. doi:10.1029/2005JA011357.

Streltsov AV, Golkowski M, Inan US, Papadopoulos KD (2010) Propagation of whistler-mode waves with a modulated frequency in the magnetosphere. J Geophys Res 115: A09209. doi:10.1029/2009JA015155.

Streltsov AV, Woodroffe JR, Huba JD (2012) Propagation of whistler mode waves through the ionosphere. J Geophys Res 117: A08302. doi:10.1029/2012JA017886.

Umeda T, Omura Y, Matsumoto H (2001) An improved masking method for absorbing boundaries in electromagnetic particle simulations. Comput Phys Commun 137: 286–299

Woodroffe JR, Streltsov AV (2013a) Whistler interactions with density gradients in the magnetosphere. J Geophys Res 118: 1–6. doi:10.1029/2012JA018308.

Woodroffe, JR, Streltsov AV (2013b) Whistler propagation in the plasmapause. J Geophys Res Space Phys 118: 716–723. doi:10.1002/jgra.50135.

Yamaguchi K, Matsumuro T, Omura Y, Nunn D (2013) Ray tracing of whistler-mode chorus elements: implications for generation mechanisms of rising and falling tone emissions. Ann Geophys 31: 665–673. 10.5194/angeo-31-665-2013

Yoon PH (2011) Large-amplitude whistler waves and electron acceleration. Geophys Res Lett 38: L12105. doi:10.1029/2011GL047893

doi:10.1186/1880-5981-66-6
Cite this article as: Katoh: A simulation study of the propagation of whistler-mode chorus in the Earth's inner magnetosphere. *Earth, Planets and Space* 2014 **66**:6.